Obstacle Detection using Optical Flow

Toby Low and Gordon Wyeth
School of Information Technology and Electrical Engineering
University of Queensland
St Lucia, Australia.
tobylow@itee.uq.edu.au, wyeth@itee.uq.edu.au

Abstract

Motion has been examined in biology to be a critical component for obstacle avoidance and navigation. In particular, optical flow is a powerful motion cue that has been exploited in many biological systems for survival. In this paper, we investigate an obstacle detection system that uses optical flow to obtain range information to objects. Our experimental results demonstrate that optical flow is capable of providing good obstacle information but has obvious failure modes. We acknowledge that our optical flow system has certain disadvantages and cannot be solely used for navigation. Instead, we believe that optical flow is a critical visual subsystem used when moving at reasonable speeds. When combined with other visual subsystems, considerable synergy can result.

1 Introduction

Navigation and obstacle avoidance are just two of biology's main instincts for survival in unknown environments. Mobile robots too must have these basic instincts integrated into their system before attempting to perform any higher-level tasks. Currently sonar and laser methods are used for obstacle detection but researchers are now looking towards an important sensory system that many biological creatures use everyday−vision.

Vision is a very powerful sensor providing numerous types of information that can be explored in many contexts for obstacle detection. Colour and texture recognition have been used to segment out the ground plane in images thus identifying free space in the forward area [Cheng and Zelinsky, 1998]. Edge obstacle detection methods have been implemented in corridor type environments due to the many straight line components and static lighting conditions [Ohya *et al.*, 1997]. Moreover edges in an image have been considered obstacles using the edge free ground plane assumption [Lorigo *et al.*, 1997] [Chao *et al.*, 1999]. All these techniques use different image aspects that have been shown to work successfully in their test environments. It is only when they are conducted in more general environments that failure occurs due to the various assumptions made. For example, texture recognition assumes the ground texture remains constant, colour recognition assumes that objects are not the same colour as the ground, and the edge detection method used in corridors requires strict model memory components plus a good simultaneous localisation and mapping (SLAM) system. In biology, it has been shown that these spatial visual systems cannot and do not function alone. Instead it suggests that these systems operate in conjunction with another important system, the visual motion system.

Visual sensors are able to sample the amalgamation of environmental motion and self-motion information of a scene through two or more successive snapshots. These snapshots encode motion at a fundamental feature level used to estimate optical flow. Optical flow can be defined by a set of vectors with each vector describing the motion of individual features in the image space. These simple vectors can provide a 2D representation of the robot's motion and the environment's 3D structure and motion under the correct conditions. As such, optical flow has been used in a many different ways for navigation and obstacle avoidance. The common ground plane segmentation using optical flow templates has been shown to be successful in identifying flat traversable surfaces [Illic and Masciangelo, 1992]. Furthermore, the use of divergence maps from optical flow fields have shown promising results with robots been seen to navigate between obstacles successfully using divergence plots [Camus *et al.*, 1999] [Nelson and Aloimonos, 1989]. Divergence and time to contact calculations for a central area have also been implemented as a frontal collision detection subsystem [Coombs *et al.*, 1995].

Evidence in biology also outlines the importance of motion with monkeys shown to contain two pathways known as Magnocellular (M) and Parvocellular (P) path-

ways [Miles and Wallman, 1993], otherwise described as being the motion and colour/texture processing pathways respectively. Insects such as bees have been shown to exploit optical flow by balancing right and left flow fields in corridor type environments [Srinivasan, 1992], and has also been proven to have great success on mobile robots [Coombs *et al.*, 1995]. No doubt visual motion is an important cue for obstacle avoidance and navigational tasks in biology. Much work has already been done on techniques for the colour/texture pathway but less so for the motion pathway.

Whilst many interesting techniques have been formed using optical flow, almost no research has been done on using optical flow to construct a simple but robust range map of the environment. Optical flow under certain conditions can provide a 3D reconstruction of the surrounding environment similar to that of stereo vision but only using one camera.

In this paper, we aim to take advantage of this 3D environmental information encoded within optical flow to extract and produce a range map. We compare this visual range map with the traditional sonar and laser sensor information and outline any improvements and shortcomings. Our approach will be slightly different to that from the known Structure from Motion (SFM) area. Instead of using the basic motion equations, we use the time to contact calculations formulated by Lee [Lee and Young, 1985] for each optical flow component. This approach was taken as the time values are hypothesised to be a key aspect in controlling mobile robots. Numerous experiments conducted by Lee [Lee, 1980] show that our actions and movements are not governed by the true time to contact but rather by the time to contact if the speed of the object were to remain constant, otherwise known as the *tau-margin*. We hypothesise that motion information is a key aspect for many functions, in particular obstacle detection, control and navigation.

1.1 Outline

In Section 2, we provide background motion information including the optical flow estimation methods and the time to contact calculations used to find the range measurements to the optical flow points. Section 3 will describe an angular Obstacle Map that is used to represent the results in addition to Cartesian space. Section 4 presents the system architecture including sensor hardware of the robot. In Section 5, errors that were encountered in optical flow will be outlined and the methods chosen to solve them presented. Section 6 describes the environmental setup, robot paths and sensors used in the experiments. Following this, Section 7 presents the results of the experiments to which Section 8 will discuss. Lastly the conclusion of this paper will be shown in Section 9.

2 Motion Framework

The motion field can be described as the projection of the 3D velocity field in a scene onto a 2D image plane and is analogous to optical flow many situations. If we let $\mathbf{P} = [X, Y, Z]^\top$ be a 3D point in the camera reference frame, Z the optical axis and f the focal length, then the image of a scene point, $\mathbf{P}$ can be mapped to the image point $\mathbf{p}$ through the following equation:

$$\mathbf{p} = f\frac{\mathbf{P}}{Z} \tag{1}$$

From this we obtain the important basic equations of motion by differentiating both sides of Equation 1 to obtain:

$$\begin{aligned} v_x &= \frac{T_z x - T_x f}{Z} - \omega_y f + \omega_z y + \frac{\omega_x xy}{f} - \frac{\omega_y x^2}{f}. \\ v_y &= \frac{T_z y - T_y f}{Z} - \omega_x f + \omega_z x + \frac{\omega_y xy}{f} - \frac{\omega_x y^2}{f}. \end{aligned} \tag{2}$$

where $\mathbf{v}$ is the velocity vector in image space, $\mathbf{T}$ is the translational velocity vector in camera space, f is focal length, Z the depth to the motion point in camera space and $\boldsymbol{\omega}$ is the rotational velocity vector in camera space.

From Equation 2, it can be seen that the rotational or translation components are linearly separable and that depth information Z for a point only exists if there is translational motion in 3D space, $\mathbf{T}$. It is from these equations that the structure from motion field is built. They give an understanding and mathematical background of the information optical flow can contain. The main difference between an optical flow field and the motion field is that optical flow only describes the apparent motion of features in an image, which may or may not correspond to the motion field.

2.1 Optical Flow Estimation

In order to extract information from an optical flow field, it must first be estimated from our images taken within a scene. There are many optical flow estimation techniques but the majority can be classified into two categories, differential or feature-based. Differential methods work using the temporal and spatial variations of all pixels in a image window and is based upon the brightness consistency equation [Trucco and Verri, 1998]:

$$(\nabla E)^\top \mathbf{v} + E_t = 0. \tag{3}$$

where $E = E(x, y, t)$ is the image brightness, $\mathbf{v}$ the motion field and the subscript t denoting partial differentiation with respect to time. This equation assumes that the apparent brightness of moving objects

remains constant and thus the change in image brightness $\Delta E(x(t), y(t), t)$ in a scene must equal zero. It is commonly solved using the least squares solution over a small patch Q, thus producing the optical flow v at the centre of the patch Q.

Feature based methods on the other hand use distinct features in image and a matching technique to find the optical flow vectors. As a consequence, the optical flow field is generally more sparse and uses less processing time than differential methods. It is for this processing time concern that a feature-based matching system was employed. Although recent studies have shown promising performances for differential techniques in closed-loop control situations [McCarthy and Barnes, 2004]. Some other advantages of using a feature-based method includes the ability to eliminate the common aperture problem as well as the ability to cope with more sporadic movements. To obtain both these advantages, corners (otherwise described as an area of large spatial changes in brightness in two different directions) are the features chosen to be tracked and matched.

Corner Detection

Corner detection is an important process for obtaining good optical flow images. There exist several corner detection methods from which the commonly known Harris corner detection method [Harris and Stephens, 1988] was chosen. It produced superior time and corner results compared to other common methods when applied to local image tests. The Harris corner detector works by using the matrix:

$$C = \begin{bmatrix} \sum E_x^2 & \sum E_x E_y \\ \sum E_x E_y & \sum E_y^2 \end{bmatrix} \quad (4)$$

where the sums of image brightness E are taken over the neighbourhood Q of point p. Corners are found by extracting the two eigenvalues of the matrix that encode the edge strengths thus producing a new matrix C:

$$C = \begin{bmatrix} \lambda_1 & 0 \\ 0 & \lambda_2 \end{bmatrix} \quad (5)$$

Thus when $\lambda_1 \geq \lambda_2$ and λ_2 is over a given threshold value, it corresponds to two strong edges in the same image window thus specifying a corner. This corner detection method was implemented using the OpenCV function *cvGoodFeaturesToTrack* as it is analogous to the Harris corner detector differing only in the threshold equation used (OpenCV uses a simple constant multiplied by the maximum eigenvalue). The OpenCV function provides adjustable variables such as the maximum corner amount to detect, threshold constant and the minimum spacing between corners found. This helps scale the number of corners found and improves spatial uniformity of the optical flow.

Matching

Matching is performed via the normalised cross correlation coefficient for a window surrounding the corners of interest found. This was implemented with the help of OpenCV's function *cvMatchTemplate* as it can be easily modified to perform other standard matching functions such as the sum of squared differences and cross correlation. With the chosen matching function, corner pairs can be eliminated using a simple threshold value ranging from 0 to 1 (1 being a perfect match). Matches are further limited with the assumption of relatively smooth movements thus should only occur in a specified search area around the position of the first corner. Once matching has been completed, the optical flow vectors can then be used to extract range information through time to contact equations.

2.2 Time To Contact

The theory of time to contact (TTC) was first introduced by Lee [Lee and Young, 1985]. Lee conducted many studies upon humans and birds showing evidence that TTC is a critical component used in the timing of motion and actions. As we fundamentally wish to develop the robot for obstacle avoidance and control, we chose to use the TTC information and believe it will help the task of obstacle avoidance at later stages. One can also simply convert these time measurements to range estimates by multiplying it by the speed of the robot for easy comparison.

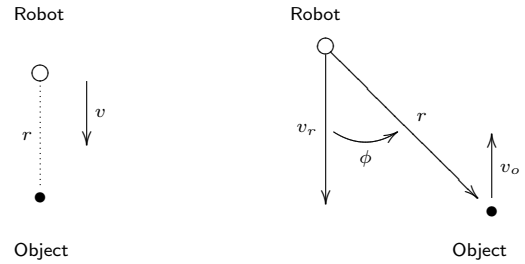

Figure 1: Time To Contact Figures: Left - Robot on a straight collision course with object, Right - Robot not on a collision course with object.

The definition of time to contact is quite simple. Given a point object travelling on a collision course with the robot, distance r from the robot and at a constant speed v (as shown in Figure 1(a)), the TTC is given by:

$$TTC = r/v. \quad (6)$$

Another way to express the TTC is to use the direction of the velocity vector v and the direction to a point

on the object [Lee and Young, 1985]. If we label the angle between these two vectors ϕ, the TTC can be alternatively calculated using:

$$TTC = \frac{cos\phi \times sin\phi}{\dot{\phi}}. \quad (7)$$

The benefit of the latter equation is that it only requires information that can be obtained purely from optical quantities. As such, this equation produces time values to each corner tracked within an image from known image-based and camera information. ϕ represents the angle between a vector r and the optical axis of the camera. It is assumed that the robot only moves in the forward camera direction and does not move perpendicular to the camera direction thus allowing simple angular calculations. This is a reasonable assumption given that the robot is of a wheelchair design and will be mainly operating in flat environments. Once each of the time to passing or contact values are found, they can be converted to range information by extracting the speed of the robot from the wheel encoders. These range vectors are then transformed into Cartesian coordinates by using the assumption of a pinhole camera model and similar triangles:

$$\begin{aligned} X &= \frac{x}{f}Z. \\ Y &= \frac{y}{f}Z. \end{aligned} \quad (8)$$

3 The Obstacle Map

Optical flow information was also used to form an Obstacle Map (OM) in order to provide a different representation of obstacle information. The Obstacle Map is a angular map with the range threshold function:

$$prox_i = f(r_i) = \frac{K_p}{r_i^2}. \quad (9)$$

where r_i is the range in metres to the point of interest i, K_p the threshold constant and $prox_i$ representing range information converted to a 0 - 1 proximity scale (1 representing the closest obstacles). As the main concern is about detecting and actuating around threatening obstacles, this type of angular range map could be much more useful for control purposes. In particular, the biological-plausible reactive navigation system developed by Browning [Browning, 2000] uses this OM combined with a Goal Direction (GD) map to produce a Motor Heading Map (MHM) that controls the direction of the robot. The method is based on the RanaC model biologically found in frogs [Arbib, 1987] and has been shown to perform well in multi-object environments [Ball, 2001].

This Obstacle Map could also be formed using time to contact information as a relative proximity measure instead of strict range information r_i. The benefit is that navigation would be purely based on optical quantities. This was to be initially implemented but to allow a fair future comparisons of the optical flow obstacle detection against traditional techniques, the strict range obstacle map format was used.

Thus through Equation 9, the OM was constructed using the Cartesian range information obtained from optical flow. As optical flow points are quite sparse and separated in feature-based estimation, an error margin of $\pm 2^\circ$ was implemented. This helps create a more smoother and continuous Obstacle Map.

4 System Architecture

The platform used to conduct the experiment was a Pioneer robot, which is developed and sold as a self-contained unit. It is a wheelchair designed robot with an inbuilt Pentium computer running a compact version of Windows XP. The Pioneer robot sensors include a sonar ring, encoders, a monocular active camera, an industry standard SICK laser and an inertial measurement unit (EiMU). The laser is located in the front area of the robot with eight (8) sonar sensors arranged beneath. The camera is mounted on top of the laser and positioned in the middle of the turning axis of the robot. An embedded motor board is used control motors and communicate encoder information back to the computer. Figure 2 shows a photo of the Pioneer mobile robot and Table 1 presents some brief information on the robot's sensors.

Figure 2: The Pioneer Robot with a SICK Laser, Sonar Ring, Active Camera and the EiMU sensor.

Sensor	Information Type	Description
Sonar	Cone projected range, 30° cone, max. range is 2m.	Consists of 8 sonar's surrounding the forward area.
Laser	Range, max. range is 150m.	Scans up to 180° with 1° angular resolution and a 10mm range resolution.
Vision	392x288 @ 25fps, 50° angular range, non interlaced image.	Provides a maximum resolution of 768x576 PAL, supports outputs in YUV, RGB and Grayscale.
EiMU	Heading $0 - 360°$, heading rate.	Consists of a single axis gyroscope and three magnetometers. Contains inbuilt software filtering and calculates heading direction with respect to magnetic north.

Table 1: Pioneer Sensor Information

5 Improving Optical Flow

There are three main problems associated with using optical flow images to obtain 3D environmental information and self-motion. Firstly, to fulfil the assumption of smooth movements, the robot has to move quite slowly and as a result produces poor and coarse optical flow data. This causes large errors in range calculations especially when sub-pixel corner finding algorithms are not employed.

The second problem is a well-known issue in computer vision, whereby any rotation or rotational disturbances will add a constant optical flow vector to each point of interest. As examined in Equation 2, rotations encode no range information thus must be removed in order to obtain the correct range information from translational movements.

Lastly, the problem of lens distortion also has an affect on the optical flow. Optical flow information is quite sensitive thus even lens distortion can alter the optical flow vectors enough to produce an incorrect observation of the motion field. It complicates the situation by changing optical flow vectors depending on the position in the image.

5.1 Tracking Corners

To help solve the problem of coarse optical flow data, we employed tracking over a number of successive images. Tracking was conducted in all directions as it produced satisfactory results with each match chosen to be tracked from either 1 to 5 images. The tracking is interleaved between images thus removing many outliers and produces a finer optical flow field suitable for range data extraction. Tracking over five successive images slows down the process of obtaining range information but the reason it is performed over five images is due to the robot moving at a slow speed. If the robot were to move at a fast pace, the number of tracking images can be reduced. This would produce the same resolution of optical flow at a faster rate (needed at higher speeds for control) but with the sacrifice of outlier reduction. Although tracking helps improve optical flow, the problem of coarse optical flow data at very slow speeds still exists. Thus we chose to ignore any information obtained from vision motion below a certain forward speed.

5.2 Rotation Removal

The area of ego-motion recovery is vast thus there exists many different algorithms to estimate rotational motion components. The problem is many of these techniques require numerous assumptions, are computationally expensive and still produce results containing errors [Giachetti *et al.*, 1998] [Gebert *et al.*, 2003]. The Pioneer robot was equipped with an EiMU[1] thus we took advantage of the in-built gyroscope to help remove rotations from the optical flow images. As the camera is aligned with the robots turning axis, rotation removal becomes the simple task of finding the heading difference in image space and subtracting it from the optical flow.

Initial tests on the EiMU presented huge errors due to the heading being fused with a reference point provided from the magnotometers. For indoor environments, large electromagnetic disturbances from computers, electrical equipment as well as from the Pioneers power and motor units affected the magnotometers greatly. Thus the magnotometers were retired and the gyroscopes rate information fused with the Pioneer wheel odometry instead. The original sensor fusion method (a complementary filter with an additional integral gain) was kept as it is simple, real-time and can easily be tweaked to combine the benefits of both datasets. Figure 3 shows a brief block diagram of the complementary filter (CF) where k_p and k_i are the specified proportional and integral gains.

To calibrate the CF, 360° rotation tests were conducted and gains tuned for a turning speed of $15°/s$. The filter results are presented in Figure 4 from which we can see the combination of the gyroscope's fine resolution and the odometry's values helping to remove gyroscopic drift.

[1] An inertial measurement unit provided by fellow researchers at the CSIRO ICT Centre.

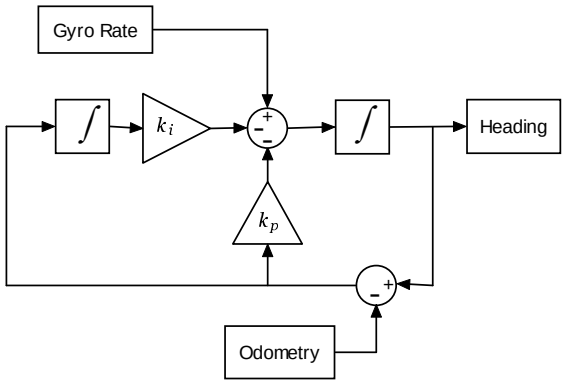

Figure 3: Complementary Filter Block Diagram for Fusing EiMU Data with Wheel Odometry.

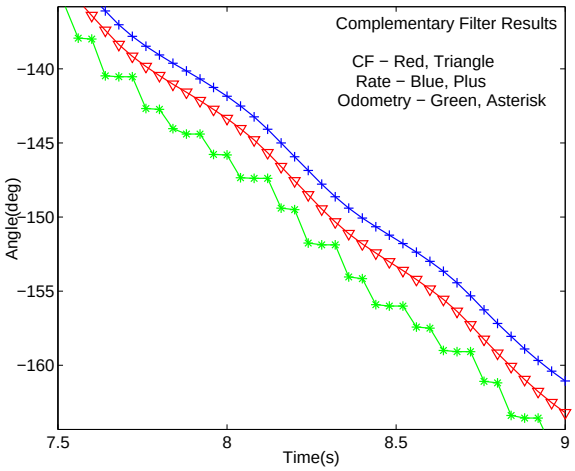

Figure 4: Complementary Filter Test Results: Complementary Filter Heading - Red/Triangle Line, EiMU Rate Integrated Heading - Blue/Plus Line, Odometry Heading - Green/Asterisk Line.

5.3 Rotation Effectiveness

In order to test the effectiveness of the rotation estimations from our CF fusion, a simple experiment that rotated the robot on the spot was conducted. If the CF rotation estimates, camera position and lens distortion model are perfect, we should obtain an optical flow image of only dots representing corners. Figure 5(a) and Figure 5(b) shows a sample of optical flow images produced before and after the rotation removal process respectively. It can be seen that a significant part of rotation components are removed with a calculated average error of 7.07% over the smooth rotation segments. This error may produce a slight shortening or lengthening effects in the range estimates but as we are concerned with obstacle detection and not precise mapping, this error level is satisfactory.

(a) Before Rotation Removal

(b) After Rotation Removal

Figure 5: Optical Flow Images of the Rotation Removal Process using the EiMU and Odometry.

5.4 Lens Distortion Removal

To remove lens distortion, camera calibration was performed via the Matlab camera calibration toolbox and distortion removed using the iterative normalisation function also provided by the toolbox. As removing distortion blurs the images slightly, we chose to normalise the points after the corners were tracked and matched up. This not only improves corner detection and matching quality levels but also speeds up the overall process; undistorting only the matching corner points instead of the whole image.

6 Experimental Setup

Two (2) experiments were conducted in order to test our the optical flow system.

1. **Straight Only** - The robot was driven forward only between two artificial obstacle targets against a very corner free background.

2. **Slow Curve** - The robot took a slow rightward curving path toward real obstacles and turns into corridor space.

The speed of the robot in the experiments ranged from 0 - 250mm/s in an area of about 5 by 3m. To gain significantly better optical flow information, speeds below 180mm/s were ignored. For comparison purposes the laser and the sonar sensor information were recorded. All tests were conducted within an office environment which was found to have a very consistent carpet colour thus producing a very corner free ground plane. It was also assumed that all corners found in an image are associated with an obstacle and considered a threat. This is a reasonable assumption since obstacles close to the robot are the main concern and due to the cameras viewing angle, any corners produced from large heights (such as the ceiling) should be classified as being relatively far away thus not affecting the closer obstacle data. Although this may not be the case in other environments such as outdoor environments, optical flow data can provide 3D information thus allowing the option of filtering values to those within the robot's height space.

7 Experimental Results

Straight line results are presented in Figure 6 and Figure 7 showing one of the better to one of the poorer frames respectively. The top-most image displays the corrected optical flow overlaying the camera image. The middle left and right images plot the optical flow and laser ranges in the same scale Cartesian space respectively. Darker dots in the left plot symbolise an obstacle of closer proximity to the robot. Note that the field of view (FOV) of the camera is limited compared to that of the laser and sonar thus only the points seen in the cameras view (top-most graph) are mapped to the Optical Flow Cartesian map. The approximate FOV limits of the camera are signified by a dotted-dashed line in each of the plots. The bottom left image shows the sonar range readings in Cartesian coordinates and the bottom right image contains the Obstacle Map created from optical flow range information (discussed in Section 3). The Obstacle Map uses an angular measure of degrees on the x-axis with the optical axis of the camera located at 180°. The FOV limits of the Obstacle Map are approximately ±28°. We chose an OM threshold value of 1.5 metres and a value of 0.5 for unknown range information. All measurements are sampled relative to the robot space with flow information obtained and tracked over a sequence of five images.

Figures 8, 9 and 10 present the curve path experiment results for frames 345, 180 and 120 respectively. These frames were chosen to give a view of the best, average and worst case scenarios respectively. The layout is identical to the straight line results except the depth axis

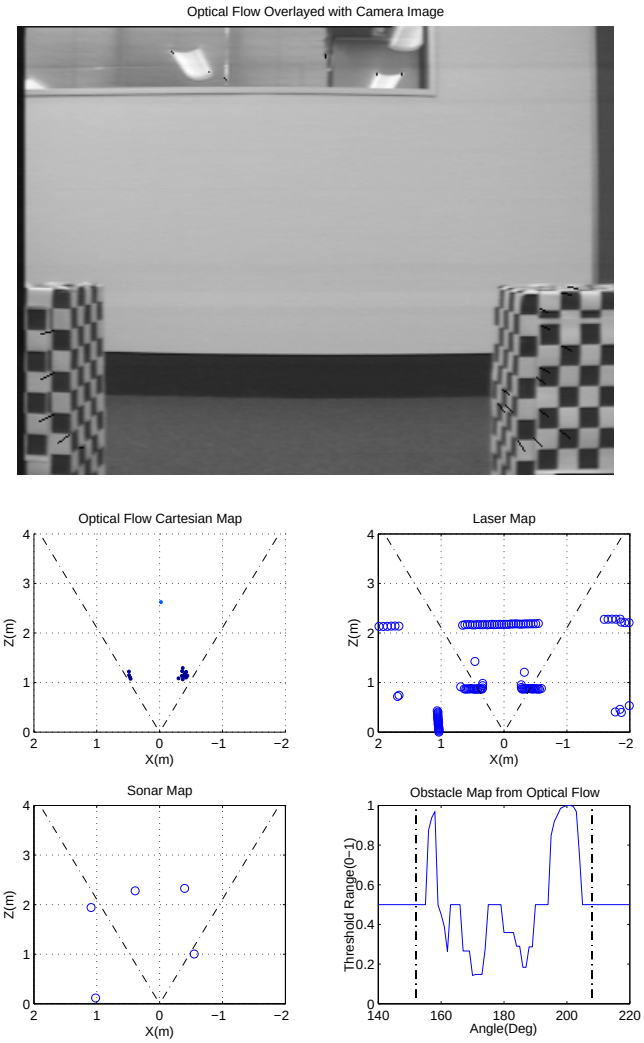

Figure 6: Experiment Results - Straight: Frame 115.

$Z(m)$ was changed from 4 to 8 metres to accommodate the long corridor measurements.

8 Discussion

Experiment 1 produced some promising results with the majority of images producing smooth flow thus providing quite accurate and consistent range information. From Figure 6, the Optical Flow Cartesian Map shows solid evidence of two obstacles with a visually inspected error of 0.2m with respect to the laser readings. This error is more than acceptable for obstacle detection as seen by the Obstacle Map which easily identifies two threatening obstacles at either side of the robot with free space between them. Comparing the vision-based method to sonar, it is seen that the optical flow information outperforms sonar with its much higher resolution map, the ability to detect the left side obstacle correctly as well providing quite accurate range information.

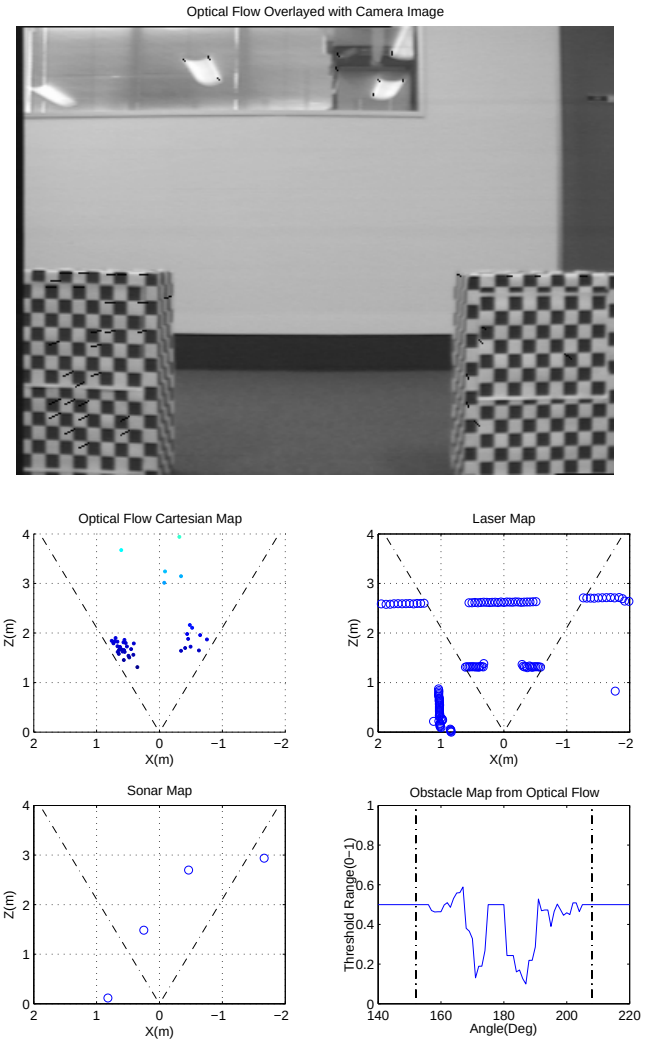

Figure 7: Experiment Results - Straight: Frame 55.

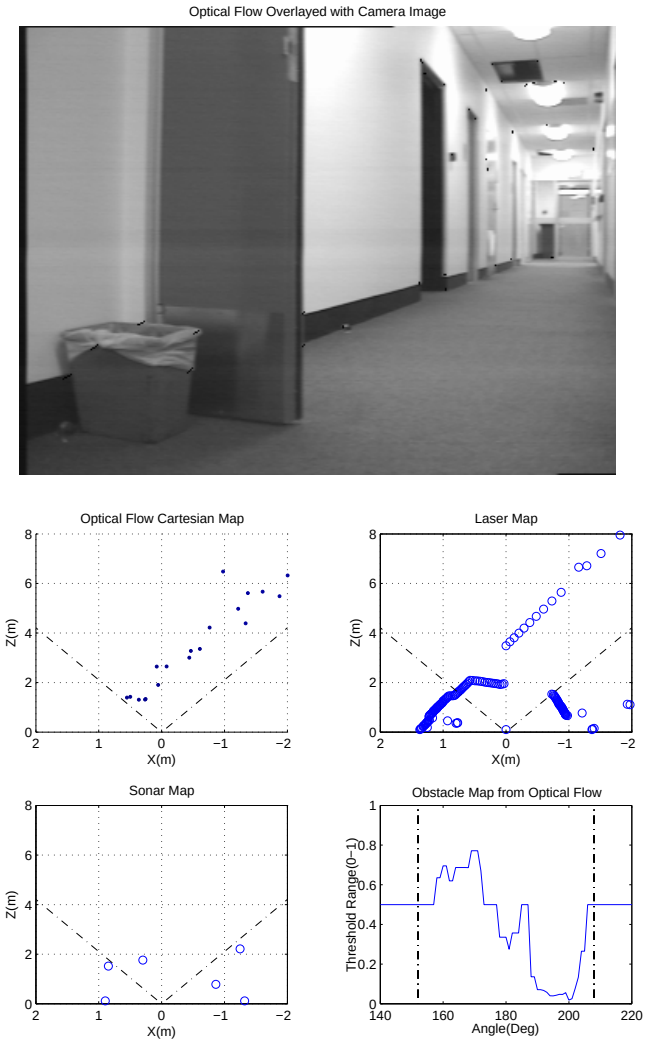

Figure 8: Experiment Results - Curve: Frame 345.

The poorer results in Figure 7 show optical flow information skewing slightly and increasing the range of the right side obstacle. Even so, optical flow range information still able to provide evidence of the right side obstacle's existence as well as the back wall.

In experiment 2, the optical flow system produced good and informative results for the majority of frames but also produced some incorrect obstacle information throughout frames 110 to 160. The better optical flow frames from the curve run (Figure 8) shows that optical flow information is able to map out the corridor wall as well as the intruding door and bin. The Obstacle Map clearly indicates the free space to the right, examined to be the corridor, and an object to the left relating to the bin and door in the overlayed image. Note that the laser map is able to pick up the other side of the door but just misses being picked up in the optical flow Cartesian map and Obstacle Map due to the camera's FOV. Comparing with sonar again, it can be seen that the detection range of optical flow is much better and although not as good as laser, is more suitable for obstacle avoidance considering the robot's maximum speed.

Figure 9 displays one of the more average optical flow results from experiment 2, with some errors produced from the doors out of focus corners as seen in the overlayed image. Regardless, the rest of the information clearly indicates the chair, some of the door and rubbish bin seen in the overlayed image.

Figure 10 shows one of the failed frames with the optical flow ranges indicating an object on a direct collision course less than 1 metre away from the robot. Further investigation revealed that the incorrect range readings were due to the sensitivity of the TTC calculations near the principle point of the image. As the angle between the pixels and principle point becomes smaller, the TTC equations become much more sensitive to any

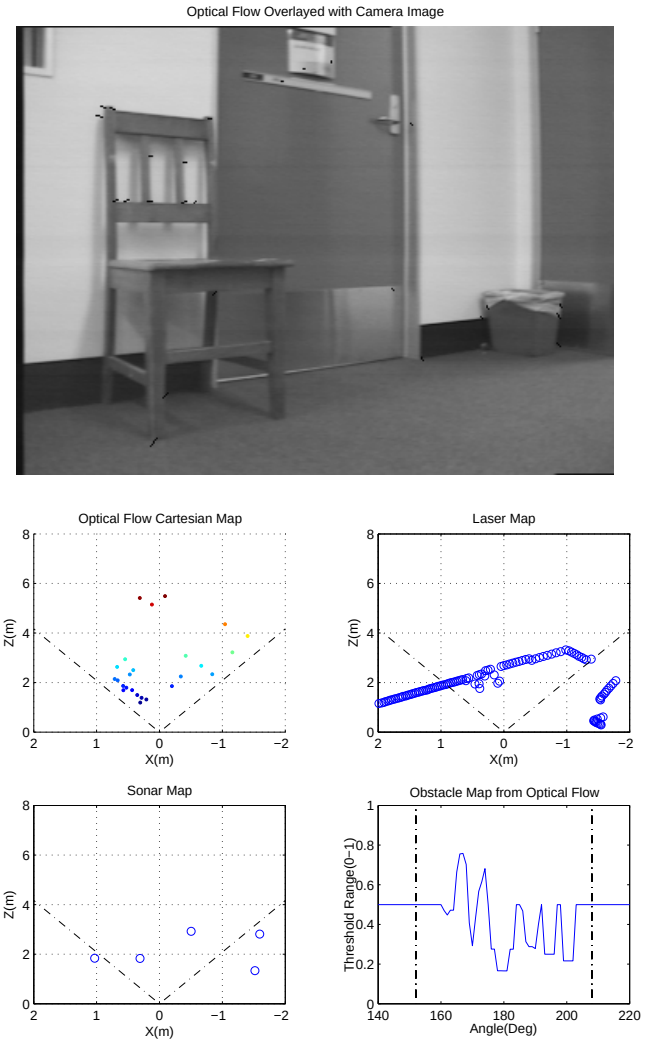

Figure 9: Experiment Results - Curve: Frame 180.

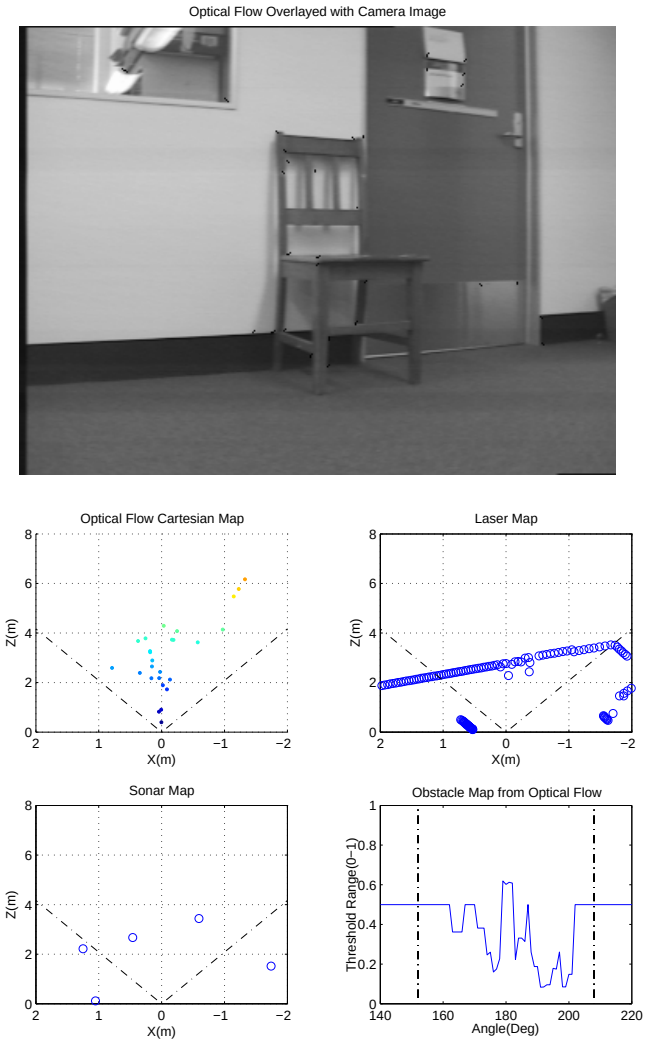

Figure 10: Experiment Results - Curve: Frame 120.

optical flow thus even small errors affect the range reading greatly. This error is further amplified as the vision system works using pixel resolution thus the coarse nature of pixel movement in the central regions only allows very discrete range readings.

This TTC sensitivity problem can be approached in numerous ways with the simplest method ignoring the central portion of the image. Another method would be to use sub-pixel interpolation or a differential optical flow technique in the central region to create finer optical flow vectors thus reducing quantisation errors. In biology, it has been investigated that monkeys and humans only focus on a central region of the image, and thus hypothesised that stereo is used to obtain depth in the central regions whereas optical flow is mainly on the outer peripheral regions of the eye. In accordance, we could also try combine this optical flow system with stereo and even colour segmentation and/or texture recognition to form a complete visual obstacle-avoidance system.

Aside from the bad frames seen in Figure 10, the optical flow obstacle detection system was relatively successful with the ability to identify and estimate ranges to obstacles given good smooth optical flow information. It was inspected in the straight line experiment and in the curve line experiment (ignoring the frames below the speed threshold) that 100% and 81% of the optical flow frames were capable of providing and locating threatening obstacle information respectively. With this percentage of consistancy seen, this technique should be able to benefit greatly from temporal filtering or path integration techniques.

9 Conclusion

In this paper, we have introduced an optical flow obstacle detection system capable of estimating obstacle positions. The CF rotation removal process and TTC

calculations employed were proven to be effective in practical situations. In many frames, the optical flow system produced range information that was on par or superior to sonar information and in some of the better frames, on par with laser information. There are some failure modes in our system; this technique was not developed to be a standalone method but a subsystem of a complete vision obstacle detection system. In summary, our results have shown that optical flow information is capable of providing useful obstacle information that can add to the strengths of other visual methods such as colour, texture and edges recognition. Motion is a critical component in biology for navigation, to which our obstacle detection system highlights the usefulness of optical flow and its promising abilities to fill the visual motion gap for mobile robots.

References

[Arbib, 1987] M. A Arbib. Levels of modeling of visually guided behavior. *Behavioural Brain Science*, 10:407–465, 1987.

[Ball, 2001] David Ball. Intelligence system for the 2001 roboroos team. Honours Undergraduate Thesis, 2001.

[Browning, 2000] Brett Browning. *Biologically Plausible Spatial Navigation for a Mobile Robot.* PhD thesis, Department of Computer Science and Electrical Engineering, The University of Queensland., 2000.

[Camus *et al.*, 1999] Ted Camus, David Coombs, Martin Herman, and Tsai-Hong Hong. Real-time single-workstation obstacle avoidance using only wide-field flow divergence. Technical report, National Institute of Standards and Technology., 1999.

[Chao *et al.*, 1999] Minn Tyi Chao, Thomas Braunl, and Anthony Zaknich. Visually-guided obstacle avoidance. *IEEE*, 1999.

[Cheng and Zelinsky, 1998] Gordon Cheng and Alexander Zelinsky. Goal-orientated behaviour-based visual navigation. *International Conference on Robotics and Automation.*, pages 3431–3436, May 1998.

[Coombs *et al.*, 1995] David Coombs, Martin Herman, Tsai Hong, and Marilyn Nashman. Real-time obstacle avoidance using central flow divergence and peripheral flow. *IEEE*, 1995.

[Gebert *et al.*, 2003] Glenn Gebert, Deryl Snyder, Juan Lopez, and Naveed Siddiqi. Optical flow angular rate determination. *IEEE*, 2003.

[Giachetti *et al.*, 1998] Andrea Giachetti, Marco Campani, and Vincent Torre. The use of optical flow for road navigation. *IEEE Transactions on Robotics and Automation.*, 14(1):34–48, February 1998.

[Harris and Stephens, 1988] Chris Harris and Mike Stephens. A combined corner and edge detector. *Proceedings of The Fourth Alvey Vision Conference.*, pages 147–151, 1988.

[Illic and Masciangelo, 1992] M. Illic and S. Masciangelo. Ground plane obstacle detection from optical flow anomalies: a robust and efficient implementation. *IEEExplore*, 1992.

[Lee and Young, 1985] David N. Lee and David S. Young. *Brain mechanisms and spatial vision.* Dordrecht and Boston and Nijhoff., 1985.

[Lee, 1980] D. N. Lee. The optic flow field: The foundation of vision. *Philosophical Transcations of the Royal Society of London. Series B, Biological Sciences.*, 290(1038):169 – 178, 1980.

[Lorigo *et al.*, 1997] Liana M. Lorigo, Rodney A. Brooks, and Eric L. Grimson. Visually-guided obstacle avoidance in unstructured environments. *IROS*, 1997.

[McCarthy and Barnes, 2004] Chris McCarthy and Nick Barnes. Performance of optical flow techniques for indoor navigation with a mobile robot. *Proceedings of the 2004 IEEE*, April 2004.

[Miles and Wallman, 1993] F.A. Miles and K. Wallman. *Visual Motion and Its Role in the Stabilization of Gaze.* Elsevier, 1993.

[Nelson and Aloimonos, 1989] Randal C. Nelson and Jhon Aloimonos. Obstacle avoidance using flow field divergence. *IEEE Transactions on Pattern Analysis and Machine Intelligence.*, 11(10), October 1989.

[Ohya *et al.*, 1997] Akihisa Ohya, Akio Kosaka, and Avia Kak. Vision-based navigation of mobile robots with obstacle avoidance by single camera vision and ultrasonic sensing. *IROS*, 1997.

[Srinivasan, 1992] Mandyam V. Srinivasan. How bees exploit optic flow: Behavioural experiments and neural models. *Philosophical Transactions: R. Soc. Lond. B*, 1992.

[Trucco and Verri, 1998] Emanuele Trucco and Alessandro Verri. *Introductory Techniques for 3-D Computer Vision.* Prentice Hall, 1998.